NASA Technical Memorandum 83751

Deposition of Na_2SO_4 From Salt-Seeded Combustion Gases of a High Velocity Burner Rig

G. J. Santoro
Lewis Research Center
Cleveland Ohio

S. A. Gökoğlu
Analex Corporation
Cleveland, Ohio

F. J. Kohl and C. A. Stearns
Lewis Research Center
Cleveland, Ohio

D. A. Rosner
Yale University
New Haven, Connecticut

Prepared for the
TMS-AIME Fall Meeting
Detroit, Michigan, September 17-19, 1984

NASA

DEPOSITION OF Na_2SO_4 FROM SALT-SEEDED COMBUSTION GASES OF A HIGH VELOCITY BURNER RIG

G. J. Santoro
National Aeronautics and Space Administration
Lewis Research Center
Cleveland, Ohio 44135

S. A. Gökoğlu
Analex Corporation
Cleveland, Ohio 44135

F. J. Kohl and C. A. Stearns
National Aeronautics and Space Administration
Lewis Research Center
Cleveland, Ohio 44135

D. A. Rosner
Yale University
New Haven, Connecticut 06520

E-2237

SUMMARY

Under the proper conditions sodium containing contaminants in the combustion air combine with sulfur impurities present in fossil fuels to deposit sodium sulfate on the blades and vanes of the hot section of gas turbine engines. Such deposits cause an accelerated metal wastage termed hot corrosion. The mechanism of deposition of Na_2SO_4 has been studied under controlled laboratory conditions and the results have been compared to a recently developed comprehensive theory of vapor deposition. Thus Na_2SO_4, NaCl, $NaNO_3$ and simulated sea salt solutions were injected into the combustor of a nominal Mach 0.3 burner rig burning jet fuel at constant fuel/air ratios. The deposits formed on inert collectors, rotating in the cross flow of the combustion gases, were weighed and analyzed. Collector temperature was uniform and could be varied over a large range by internal air cooling. Deposition rates and dew point temperatures were determined. Supplemental testing included droplet size measurements of the atomized salt solutions. These tests along with thermodynamic and transport calculations were utilized in the interpretation of the deposition results.

INTRODUCTION

Hot corrosion is a life-limiting form of accelerated environmental attack that can occur on vanes and blades in the hot section of combustion turbine engines (refs. 1 to 3). It is generally agreed that deposits of sodium sulfate, often in synergistic combination with low levels of elements such as potassium, vanadium, carbon, lead and particles or vapors of sodium chloride, are capable of compromising the protective oxide scales formed on engine components and of sometimes preventing the reforming of a protective scale (ref. 4).

Examples of deposition modes cited in the literature, occurring in service or in service-simulating rigs, include the work of Jackson (ref. 5), who used an air-cooled probe to study deposit formation in residual fuel-oil-fired boilers. Jackson concluded that the dominant mode of deposition was vapor diffusion of NaOH or Na_2SO_4 across the boundary layer. Steven and Tidy (ref. 6), using an industrial gas turbine simulator, concluded that deposition occurred through vapor mass transfer of NaOH or NaCl across the boundary layer. These species were assumed to be converted to Na_5SO_4 in the boundary layer at the test surface. Using an industrial gas turbine simulator, Vermes (ref. 7) concluded that the fifteen fold increase in deposition rate in a cooled cascade as compared with the case of an adiabatic cascade can be attributed to thermophoresis versus eddy diffusion modes of deposition for the two cases, respectively.

An objective at NASA Lewis Research Center is aimed at developing a rational simulation criteria for laboratory testing of high temperature materials for gas turbine engines. Toward this end a study was initiated to determine the deposition rates of sodium sulfate deposits from sodium salt-seeded combustion gases of a well instrumented high velocity burner. Thus Na_2SO_4, NaCl, $NaNO_3$ and simulated sea salt solutions were injected into the combustor of a Mach 0.3 burner rig operating at constant fuel/air ratios. The deposits formed on an inert collector rotating in the cross flow of the combustion gases were weighed and analyzed. The collector temperature was uniform and could be varied over a large range by internal air impingement cooling. The experimental results were compared to Rosner's vapor diffusion theory (ref. 8 to 13) as a means of acquiring insight into the transport, aerodynamic and thermodynamic conditions prevailing under these test conditions. The interpretation of the deposition results was aided by supplemental testing, including droplet size distribution of the atomized salt spray introduced into the combustor.

Primary Experimental Procedures

The burner rig is shown in figure 1 and the internally air-cooled collector in figure 2. A schematic representation of the flow systems are given in figure 3. The collector is a Pt-20 percent Rh cylinder with an o.d. of 1.9 cm (3/4 in.) and a height of 1.3 cm (1/2 in.). It has a 0.6 cm (1/4 in.) deep vertical hole in its 0.3 cm (1/8 in.) thick wall for accepting a thermocouple. Above and below the collector are 1.9 cm (3/4 in.) o.d. by 3.8 cm (1.5 in.) long ceramic tubes (spacers). The lower spacer contains a longitudinal groove to accommodate the ceramic-sheathed thermocouple leads. Within the cylinder formed by the collector and its ceramic spacers is an inconel tube, closed at the top and perforated with small holes through which cooling air impinges on the inner wall of the collector. The collector and the spacers are spring loaded to allow for thermal expansion and to assure intimate contact of the enclosed thermocouple junction within the collector wall. This collector assembly design allowed deposition runs to be conducted at constant combustion gas temperatures (constant fuel/air ratios) while the collector temperature was varied over a wide range, from beyond the dew point temperature of the deposit down to 500° C. The enclosed thermocouple in the collector not only measures the temperature of the collector, but is also used as a signal source to operate a closed-loop cooling air flow control system. A thermocouple located downstream of the collector provides the necessary signal for the closed-loop fuel flow control system. The combustion air flow valve is set manually to provide a gage pressure of 6.9 kPa (1 psig) within the burner. The combustion

air flow and fuel flow are measured by calibrated turbine flowmeters. The maximum flows are 2.1 ml/sec (2 gal/hr) of fuel and 37.8 g/sec (300 lb/hr) of air. The salt solution is pumped into the combustor by a peristaltic pump at a calibrated flow rate. The solution is air atomized into a fine spray within the combustion chamber downstream of the ignitor and 10.8 cm (4 1/4 in.) upstream of the throat of the exit nozzle of the burner.

Preliminary testing to completely checkout the system has been presented elsewhere (ref. 14). These tests include deposition rates for various collector temperatures, salt solution concentrations and flows, collector rotation speeds and fuel/ air ratios. The common testing parameters used for the present experiments were the internally cooled Pt-Rh collectors (7.6 cm^2 area) located 1 cm from the exit nozzle, 30-minute runs (at temperature with salt), collector rotation at 230 rpm, a salt solution flow rate of 200 ml/ hr and 34 kPa (5 psig) atomizing air pressure. The burner was individually seeded with Na_2SO_4, synthetic sea salt, NaCl and $NaNO_3$. The concentration of the sodium in each salt with respect to the combustion air was about 6.5 ppm by weight. Following each run, the deposit was weighed and subsequently analyzed. Some runs were conducted with preheated combustion air. Specific parameters for each salt are listed in table I.

To provide insight into the deposition process occurring in this burner rig, the experimental deposition rates were compared to those predicted by Rosner's Chemically Frozen Boundary Layer (CFBL) theory of vapor diffusion. Briefly the theory predicts a deposition flux resulting from simultaneous Fick (concentration) diffusion, Soret (thermal) diffusion, convection, and turbulence across a gaseous boundary layer between the combustion gases and the surface of the collector. Thermodynamic equilibrium is assumed to exist at the outer and inner edges of the boundary layer. The boundary layer is assumed to be chemically frozen or "source free." This means that no chemical reaction, condensation, nucleation, or coagulation occurs within this layer. All the sodium added to the combustion gases is available for transport to the collector via vapor species, e.g., NaCl, NaOH, Na and Na_2SO_4. The mass flux for each such species, i, at the surface is given by

$$-J''_{i,w} = \Gamma_{turb} \frac{(D_i \rho)_\infty}{L} \Gamma_{i,Soret} Nu_{m,i} \times (W_{i,\infty} - W_{i,w}) - B_{T,i} \frac{\Gamma_{ncp}}{\Gamma_{i,Soret}} W_{i,w} \quad (4)$$

The CFBL theory is capable of handling vapor and heavy-molecule deposition modes, which covers the service type examples discussed in the introduction. Thus in contrast to previous treatments of vapor deposition (refs. 15 and 16), the CFBL theory makes explicit provision for the effect of element transport of species of different mobility, thermal (Soret) diffusion, free-stream turbulence intensity and scale, and variable gas properties across the gaseous boundary layer. Further details of the CFBL theory are provided in the references (refs. 10 and 11) and the recently complied CFBL computer manual (ref. 17). A simplified hand calculated example of the theory is also available (ref. 14).

Primary Experimental Results

The data for the Na_2SO_4 - seeded burner runs are given in figure 4. The dash curve represents the CFBL predicted rates. Table I summarizes the CFBL computer program input and results. A 57 percent disparity in the plateau levels exists between theory and experiment for the Na_2SO_4 case. Here and in all the single component salt-seeded runs lower experimental deposition rates are observed at collector temperatures above the melting point of Na_2SO_4 (884° C). The data tended to tail off toward the dew point temperature.

Deposition rates on collectors exposed to synthetic sea salt-seeded combustion gases are given in figure 5. The composition of the sea salt meets the ASTM standard, ASTM D-1141-52. The sea salt case is more complex than a single-component solution as more than one species can deposit. The data points represents the sum total of these deposits, while the dash curve represents the predicted rates for Na_2SO_4 only. Under the conditions of these experiments, the bulk of the deposit is expected to be Na_2SO_4. A representation of the relative deposition rates for all components of the deposit based on conditions similar to those listed in table I for sea salt is given in figure 6. The dew point and transistion temperatures were calculated by the NASA Complex Chemical Equilibrium Computer Program Code (CEC) (ref. 18), without considering transport through a boundary layer. This procedure should yield a rough approximation of relative deposition rates provided the transport properties of the vapor species containing the elements of the condensed phases are of the same order of magnitude. The X-ray diffraction (XRD) analyses of the deposits on the collectors exposed at 550°, 650°, 750° and 850° C revealed the presence of Na_2SO_4 and MgO. The MgO intensities decreased relative to those of Na_2SO_4 with decreasing collector temperature. But MgO was still present in deposits at the two lowest collector temperatures (500° and 600° C), where according to figure 6, $MgSO_4$ should be the stable magnesium phase.

Apparently the kinetics are such that condensed MgO, which is stable at the combustion gas temperature, does not convert to $MgSO_4$ at the collector temperature in the given time frame. Energy Dispersive Spectroscopy (EDS) analyses of the deposit on the collectors exposed at 500° and 950° C revealed those elements expected from figure 6, including potassium in the 500° C deposit. In the latter, however, the EDS spectrum also displayed weak intensity K_α and K_β lines for chlorine.

Figures 7 and 8 show the NaCl and $NaNO_3$ results, respectively, along with the CFBL predictions. In both cases only Na_2SO_4 was detected by XRD. There is a definite indication in the $NaNO_3$ data of a maximum in the rate curve at about 850° C, for which there exists no ready explanation. The plateau experimental deposition rates of the NaCl runs agree very well with the predicted values.

Although all the deposition runs were conducted with about the same seed level of sodium and all other test parameters were comparable, a significant lowering of the Na_2SO_4 dew point temperature is predicted for the NaCl and sea salt runs due to the presence of NaCl vapors in the combustion gases. This dew point shift is not readily apparent by comparing the experimental deposition rate curves as they tended to tail off in the vicinity of the dew point in the single component runs.

Supplmentary Test Procedures and Results

Deposition of Liquid Na_2SO_4. - The deposition rates for Na_2SO_4 above its melting point are lower than anticipated, suggesting that not all of the liquid condensate is remaining on the collector. Several possible loss mechanisms were investigated: (1) liquid flow from the collector to the adjacent spacers; (2) spalling during the liquid to solid phase transition when the collector is cooled upon completion of the run; and (3) blow off of the liquid deposit by the aerodynamic shear forces of the high velocity burner gases. To test the first possibility, collectors with Na_2SO_4 deposit applied at collector temperatures well below the 884° C melting point of Na_2SO_4 were reinserted into the rig with virgin spacers and exposed to unseeded burner gases at collector temperatures above 884° C. Subsequent analyses of the spacers detected no sodium indicating the absence of deposit flow from the collectors. To test the second possibilty, a collector with Na_2SO_4 deposited in the same manner as in the previous procedure was placed in a weighed platinum crucible and heated in a furnace at 900° C. No indication of spalling was observed when the collector was removed from the furnace. To test the third possibility, it was reasoned that the liquid deposit may be retained if the surface of the collector were rough or porous. A collector composed of a thin layer of ceramic material on a metallic substrate could provide such a surface and yet allow for internal cooling. A thermal barrier coating of yittria stablized zirconia with a suitable bond coat on a stainless steel substrate would apparently meet these requirements (ref. 19). Such collectors were fabricated to the same dimensions as the PT-Rh collectors and exposed to salt-seeded combustion gases at collection temperatures above the melting point of Na_2SO_4. The deposit was analyzed for sodium by Atomic Absorption Spectroscopy (AAS). The deposition rates using the ceramic coated collectors are shown in figure 4 to be at the plateau level of the experimentally observed deposition rates. The temperature range assigned to the ceramic coated collector data reflects the temperature gradient observed from its windward surface to its leeward surface, even though the collectors were rotating at 230 rpm.

The experimental results depicted in this section suggest that liquid deposits of Na_2SO_4 are blown off the surface of the smooth Pt-Rh collectors in the high velocity gas stream, but are retained on a rough or porous surface. A theoretical treatment of liquid flow due to aerodynamic shear has been developed by Rosner et al. (refs. 20).

Temperature Distribution on a Stationary Collector

A rotating cylinder totally immersed in a crossflow gas stream should not display the temperature gradient observed with the ceramic coated collector discussed in the previous section. The leeward cooling could be caused by the entrainment of ambient air, which would occur if the diameter of the cylinder were large compared to the jet diameter. In the calculation of the mass transfer Nusselt number for each sodium species, a cylinder in cross flow was assumed. The calculation used the equation,

$$Nu_{m,i} = (0.4\ Re^{1/2} + 0.06\ Re^{2/3}) \times Sc_i^{0.4} \left(\frac{T_o}{T_w}\right)^{-0.04} \qquad (2)$$

An angular temperature variation around the cylindrical collector would not only invalidate the value of the calculated Nusselt number, but it would also effect the mainstream concentration of the sodium species around the collector. Because the diameter of the collector, 1.9 cm (3/4 in.), is fairly large relative to the diameter of the throat of the burner nozzle, 2.54 cm (1 in.), the cross flow assumption required verification. For this purpose an uncooled stationery Pt-Rh collector was exposed to unseeded combustion gases under the same aerodynamic conditions used in the deposition experiments. Figure 9 presents the temperature distribution around the circumference of the collector. The 255° C temperature gradient from windward to leeward surfaces demonstrates that the collector was too large to be totally immersed in the gas stream thus allowing the entrainment of ambient air. The cross flow assumption thus is not valid for this experimental setup, and the values used for Nu_m and $W_{i,\alpha}$ were inaccurate.

Droplet Size Distribution

It has been assumed until now that all of the salt sprayed into the combustor completely vaporized. In light of the discrepancy between the predicted and experimental deposition rates, that assumption has to be examined. The realization that inaccurate values were used for Nu_m and $W_{i,\alpha}$ is not sufficient to account for the differences between theory and experiment. The magnitude of the difference varies, from 57 percent for Na_2SO_4 down to 3 percent for NaCl. Thus the difference is not independent of the salt as would be expected for a systematic error in the calculations. An alternative explanation would be the existence of salt droplets large enough to inertially impact. Since the salts would vaporize at different rates, the final droplet sizes reaching, the collector would vary, resulting in different deposition rates for each salt.

To determine if the residence time of this salt in the combustion gases is sufficient for complete vaporization, it is necessary to know the size distribution of the salt solution spray injected into the combustor. The droplet size distribution of the salt solution spray was measured at various atomizing air pressures with a Melvern droplet size analyzer, a two mW HeNe laser device that utilizes the Fraumhofer diffraction principle (ref. 21). The droplet size distribution for distilled water and the dilute salt solution (~6 g/l) were all within experimental error, so the data representing the mean droplet diameter as a function of atomizing air pressure was combined into one curve, figure 10. A typical size distribution histogram is also given. The Sauter Mean Diameter (SMD) was taken as the characteristic mean of the distribution. The SMD is the diameter of a monodispersoid having the same surface area as the given spray. In determining the time for complete vaporization of this characteristic solution droplet (37.5 μm), it was assumed that the water in the solution droplet would vaporize first, leaving just the salt, which would form a molten droplet whose diameter would be related to its density, its original concentration in the solution and the solution droplet diameter. This modeling leads to a conservative estimate of the vaporization time. An alternate and less tractable model would be an initial vaporization of the water until the remaining water becomes superheated and the explosion of the droplet into an indeterminant distribution of smaller droplets, leading to a shorter vaporization time. Using the conservative approach, the time to completely vaporize just the water form the SMD droplet was calculated to be about 6 msec. The method used in the calculation has been presented elsewhere

(ref. 14). But the residence time of the spherical droplet in the combustor is 2.3 msec. Thus there isn't even enough time in the combustor to completely vaporize the water from the solution droplet. Had the water been completely vaporized, the diameter of the resultant molten salt droplet would have been about 5 μm, large enough to inertially impact under the condition of these experiments. These calculations suggest that inertial inpaction occurs in all the deposition runs, regardless of which salt is injected into the combustor. An inertial impaction mechanism may explain deposition rates greater than those predicted by the vapor diffusion theory.

Particle Capture Tests

Whereas the previous section rationalizes the discrepancies between the experimental deposition rate data and the vapor diffusion theory predictions, it is imperative to experimentally verify the existence of particles in the gas stream at the collector station. Therefore, particle capture tests were conducted. Platinum targets on a water cooled copper support were exposed for a few seconds to Na_2SO_4 and NaCl seeded combustion gases of the burner rig operating under typical deposition test parameters. The targets were positioned at the same distance from the nozzle as in the deposition runs, i.e., about one cm from the nozzle of the burner. The targets were examined in the SEM. Particles were detected for both salts and their elemental composition was determined by EDS scans, see figure 11. In the Na_2SO_4 case a very wide size distribution was observed, ranging from submicron to diameters as large a 67 μm. Only sodium and sulfur and the platinum background were detected in the EDS scans. A much narrower size distribution was observed for the NaCl tests, from submicron to about three microns. Sodium and chlorine lines were observed in the EDS scans. It will be recalled that only Na_2SO_4 was detected by XRD in the deposits of the NaCl-seeded deposition runs. The deposition rate runs lasted 30 min. In the particle capture tests targets were exposed to the salt seeded combustion gases for about three seconds for NaCl and about 10 sec for Na_2SO_4. The presence of chlorine in the NaCl test suggests that in the deposition rate runs, NaCl particles were deposited but, because of their small size, they were quickly converted to Na_2SO_4. Only the NaCl particles deposited very near the completion of the run would remain unconverted. The amount of unreacted NaCl would be too small to be detected by XRD.

The deposition mechanism for the $NaNO_3$ case can be inferred from the experience with Na_2SO_4 and NaCl, i.e., $NaNO_3$ is deposited as small particles by inertial impaction. These decompose and then reacts with the sulfur in the combustion gases to form Na_2SO_4. Only the last particles of $NaNO_3$ to deposit remain as the nitrate. The deposition mechanism from sea salt seeded runs would be a combination of the individual NaCl and Na_2SO_4 cases, in addition to the deposition of minor amounts of nonsodium compounds.

Discussion

Recently McCreath (ref. 22) has discussed three major factors that might account for discrepancies, observed in high temperature corrosion results obtained in gas turbine engines and experimental engine simulation rigs. These factors include: (1) the way salt is introduced into the combustor, its losses from the components within the rig and its history and physical state from the point of injection to the time it reaches the specimens; (2) the chemistry of

the combustion gases, including the completeness of the combustion reaction; and (3) the aerodynamic character of the flow and the specimen geometry. All of these factors (experimentally and/or theoretically), have been considered to varying degrees in this report and in the previously published related paper (ref. 14), with respect to the deposition of sodium sulfate.

The aerodynamic aspects of gas turbine blade corrosion has been summarized by Moore and Crane (ref. 23), including a section on deposition mechanism. These authors suggest that the primary mechanisms of particle delivery in gas turbines are inertial impaction, turbulent eddy diffusion, Brownian diffusion and thermophoresis. Which mechanism predominates depends on the size of the particles entrained in the combustion gases and aerodynamics. The relationship between particle size and relative deposition rates has been predicted by Rosner and Fernandez de La Mora (ref. 12) and is reproduced here (slightly modified) as figure 12. It is seen that when inertial impaction occurs, its contribution to the amount of deposit overwhelms that contributed by vapor or particle diffusion. The importance of thermophoresis in enhancing the deposition rate is also evident.

The distribution of particle sizes observed in the particle capture tests suggests that all the modes of deposition discussed above are operable in the deposition rate data presented here. However, inertial impaction of particles is probably the dominant mode.

Even in the absence of the wide distribution of particle sizes, i.e., all vapors or monodispersoids of particles small enough to diffuse, our predictive capabilities via the CFBL equation would still be hindered by the large collector dimension relative to the size of the gas stream jet. Nevertheless our ability to reproducibly deposit Na_2SO_4 under controlled aerodynamic conditions and to qualitatively relate deposition rate to the sodium salt seeded into the combustor, presents the possibility of correlating corrosion rates with deposition rates.

The implication is that burner rigs may possibly be employed in meaningful corrosion mechanism studies. These studies may be conducted with a degree of control of the experimental parameters and confidence in interpreting the results, approaching that realized in furnace tests. However, mechanistic studies in burner rigs would be more realistic because they include the effects of high gas velocities and continuous deposition of the corrosive salt.

NOMENCLATURE

B_T	dimensionless thermal diffusion (thermo phoresis) parameter
D	Fick (Brownian) diffusion coefficient
F_{ncp}	correction for variable (nonconstant) properties within boundary layer
F_{Soret}	correction factor for thermal diffusion
F_{turb}	correction factor for main stream turbulence
j''	diffusion mass flux
L	characteristic collector dimension

Nu	Nusselt number
Re	Reynolds number
Sc	Schmidt number
T	absolute temperature
ρ	density
ω	mass fraction in gas mixture

Subscripts

i	species
m	mass transfer
o	stagnation conditions
w	gas side of interface (wall)
∞	gas stream outside of combustor unaffected by collector

REFERENCES

1. J. Stringer: in Annual Review of Material Science, R. A. Huggins, R. H. Bube and R. W. Roberts, eds., pp. 477-509, Annual Reviews, Pal Alto, CA 1977.

2. Hot Corrosion Problems Associated with Gas Turbines, Special Technical Publication No. 421, ASTM, Philadelphia, PA, 1967.

3. G. A. Whitlow, S. Y. Lee, P. R. Mulik, R. A. Wenglarz, T. P. Sherlock and A. Cohn: Proceedings of the EPRI/DOE Second Conference on Advanced Materials for Alternative Fuel-Capable Heat, pp. 4-73 - 4-107, EPRI, Palo Alto, CA, 1982.

4. J. Stringer: Proceedings of the First Conference on Advanced Materials for Alternative-Fuel-Capable Directly Fired Heat Engines, John M. Fairbanks and John Stringer, eds., pp. 331-339, CONF-790749, 1979.

5. P. J. Jackson: Ash Deposits and Corrosion Due to Impurities in Combustion Gasses, R. W. Bryers, ed., pp. 147-161 Hemisphere Publishing, Washington, DC, 1978.

6. C. G. Stevens and D. Tidy: J. Inst. Energy, 1981, vol. 54, pp. 3-11.

7. G. Vermes: J. Eng. Power, 1979, vol. 101, pp. 542-548.

8. F. J. Kohl, G. J. Santoro, C. A. Stearns, G. C. Fryburg and D. E. Rosner: J. Electrochem. Soc., 1979, vol. 126, pp. 1054-1061.

9. D. E. Rosner: PCH/Physico Chemical Hydrodynamics, 1980, vol. 1, pp. 159-185.

10. D. E. Rosner, B.-K. Chen, G. C. Fryburg and F. J. Kohl: Combust. Sci. Technol., 1979, vol. 20, pp. 87-106.

11. S. A. Gökoğlu and D. E. Rosner: Int. J. Heat Mass Transfer, 1984, vol. 27, pp. 639-646.

12. D. E. Rosner and J. F. DeLaMora: Proceedings of the First Conference on Advanced Materials for Alternative-Fuel-Capable Directly Fired Heat Engines, John M. Fairbanks and John Stringer, eds., pp. 301-330. CONF-790749, 1979.

13. D. E. Rosner, K. Seshadri, J. F. DeLaMora, G. C. Fryburg, F. J. Kohl, C. A. Stearns and G. J. Santoro: Characterization of High Temperature Vapors and Gasses, J. W. Hastle, ed., Special Publication No. 561/2, pp. 1451-1476, NBS, Washington, 1979.

14. G. J. Santoro, F. J. Kohl, C. A. Stearns, S. A. Gokoglu and D. E. Rosner: NASA-TP-2225, March 1984.

15. C. G. McCreath: Proceedings of the Third Conference on Gas Turbine Materials in a Marine Environment, Session V. Paper No. 2, University of Bath, England, 1976.

16. K. Ross: J. Inst. Fuel, 1965, vol. 38, pp. 273-277.

17. S. A. Gökoğlu, B.-K. Chen and D. E. Rosner: "Computer Program for Multicomponent Convective Diffusion Deposition Rates from Chemically Frozen Boundary Layer Theory," Analex Corp., Cleveland, and Yale University, January, 1984. (NASA-CR-168329).

18. S. Gordon and B. J. McBride: NASA SP-273, March 1976.

19. S. Stecura: Private Communication, June 1983.

20. D. E. Rosner, D. Guenes and N. Nazih-Anous: Chem. Eng. Commun., 1983, vol. 24, pp. 275-287.

21. J. Swithenbank, J. M. Beer, D. S. Taylor, D. Abbot and C. G. McCreath: Experimental Diagnostics and Gas Phase Combustion Systems, B. T. Zinn, ed., pp. 421-447, AIAA, New York, 1977.

22. C. G. McCreath: Corros. Sci., 1983, vol. 23, pp. 1017-1023.

23. M. J. Moore and R. I. Crane: Deposition and Corrosion in Gas Turbines, A. B. Hart and A. J. B. Cutler, eds., pp. 34-57, Applied Science, New York, 1973.

TABLE I. - CFBL COMPUTER PROGRAM. INPUT DATA AND RESULTS

	Species			
	Na_2SO_4	Sea Salt	NaCl (preheated air)	$NaNO_3$ (preheated) air)
Airflow, kg/hr (lb/hr)	72.1(158.9)	73.6(162.2)	67.0(147.6)	66.8(147.2)
Inlet air temperature, K	298	298	532	532
Fuel-to-air ratio	0.0481	0.0465	0.0465	0.0466
Sulfur concentration in fuel, percent	0.052	0.052	0.048	0.061
Salt concentration in air, ppm (weight)	18.7	22.7	17.0	23.2
Sodium concentration in air, ppm (weight)	6.05	6.87	6.69	6.28
Adiabatic temperature, T_A, K	1886	1845	2001	2003
Stagnation temperature, ($T_O = T_A - 150^\circ$ C),[a] K	1736	1695	1851	1853
Dew point temperature,[b] K	1310	1255	1262	1312
Plateau deposition rate (experimental), $\dot{m}$, mg/hr	26.9±2.7	17.6±2.0	12.9±1.8	15.8±3.3
Plateau deposition rate (CFBF), $\dot{m}$, mg/hr	11.7	13.5	12.5	11.8
Difference between experimental and CFBL plateau deposition rates, percent	57	23	3	25

[a]Actual combustion gas temperatures averaged 150° C below the adiabatic temperatures calculated from fuel-to-air ratios.
[b]Calculated by using CEC code.

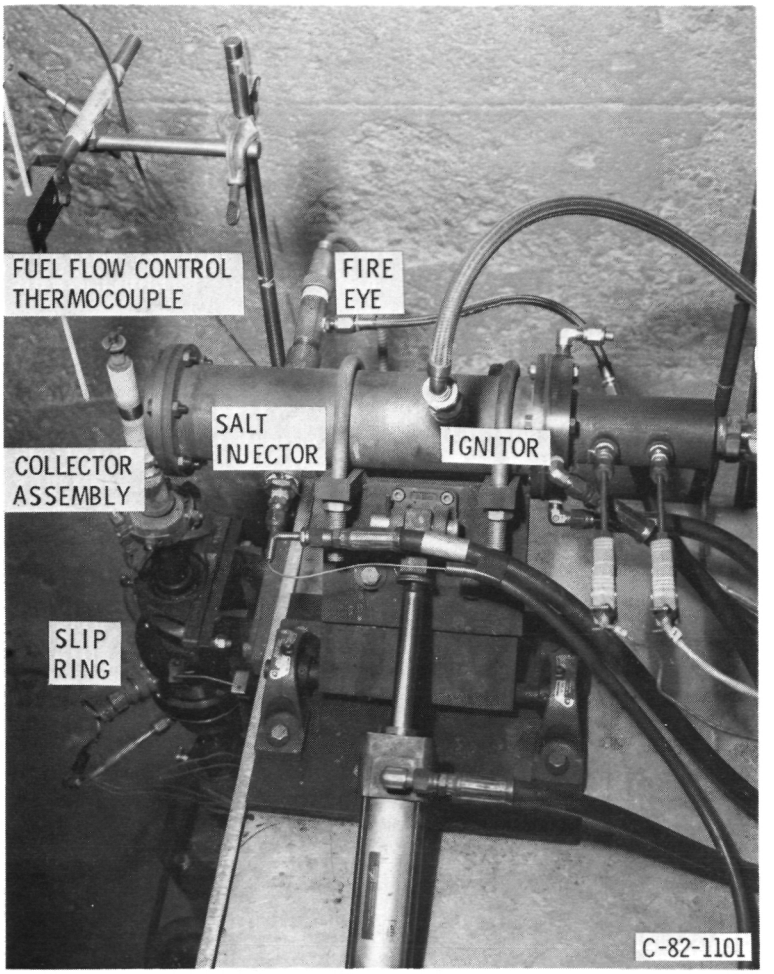

Figure 1. - Burner rig deposition configuration with internaly cooled collector and salt solution injector.

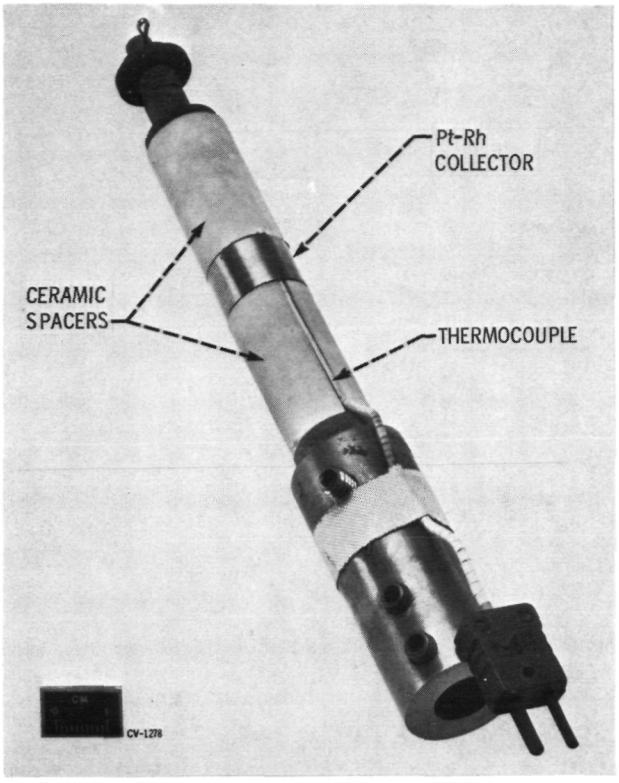

(a) Assembled collector

Figure 2. - Internally cooled collector. Cooling is effected by impingment of air from small holes in the center stem onto the inner wall of the collector.

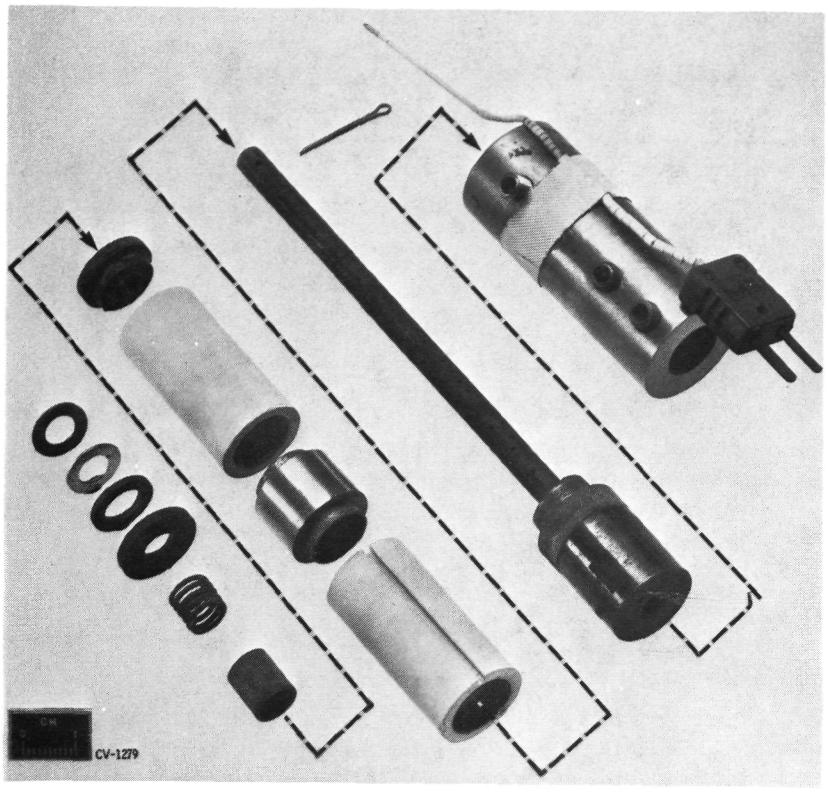

(b) Exploded view

Figure 2. - Concluded.

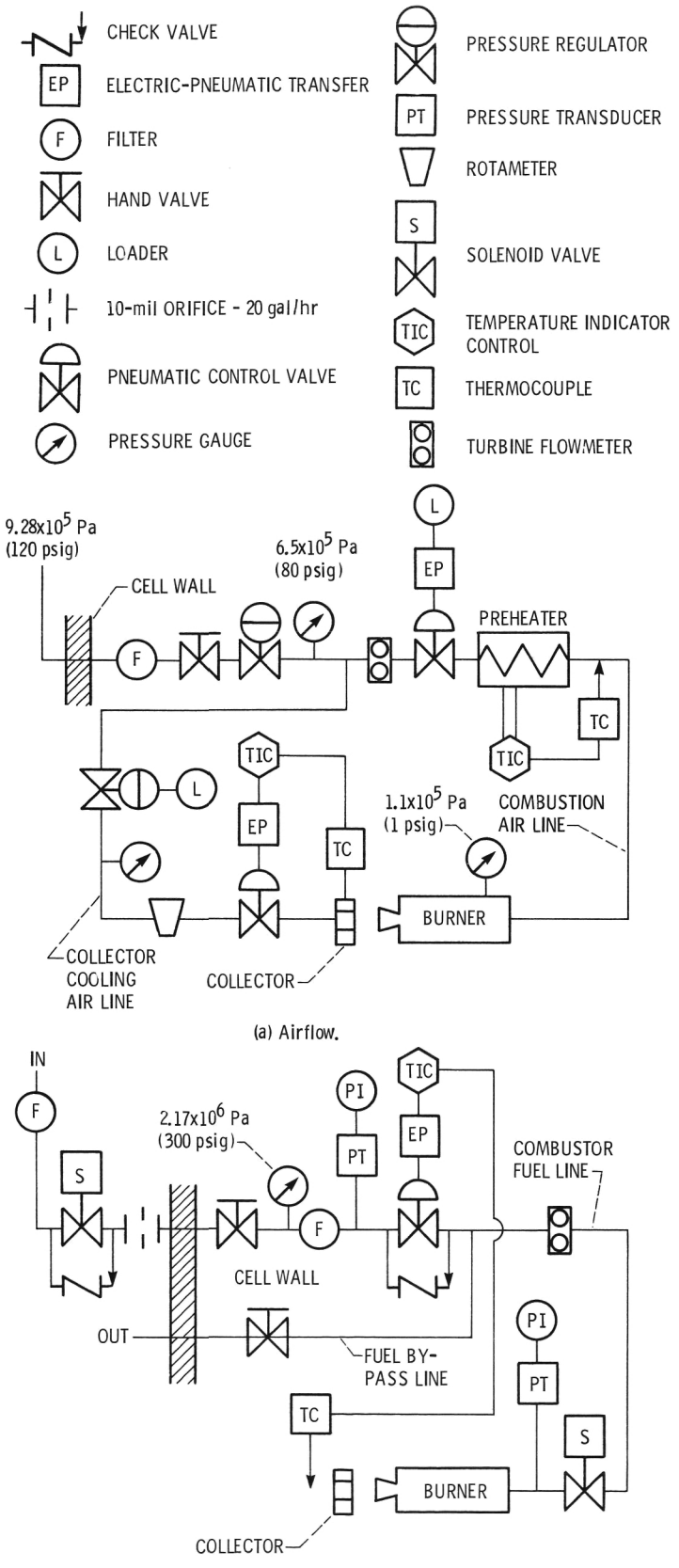

Figure 3. - Simplified schematic representation of the flow systems and controls.

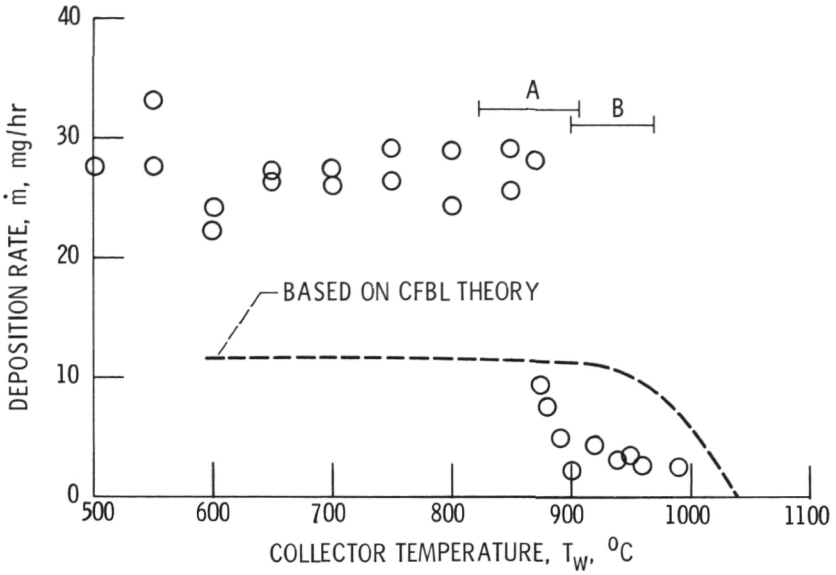

Figure 4. - Effect of collector temperature on deposition rate from Na_2SO_4-seeded combustion gases. Bracketed data are the deposition rate results on ceramic-coated collectors A and B.

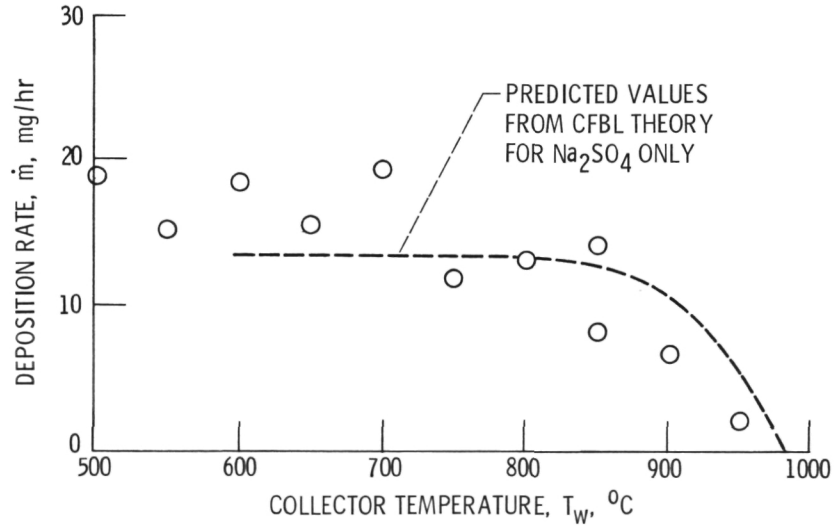

Figure 5. - Effect of collector temperature on deposition rate from synthetic-sea salt-seeded combustion gases.

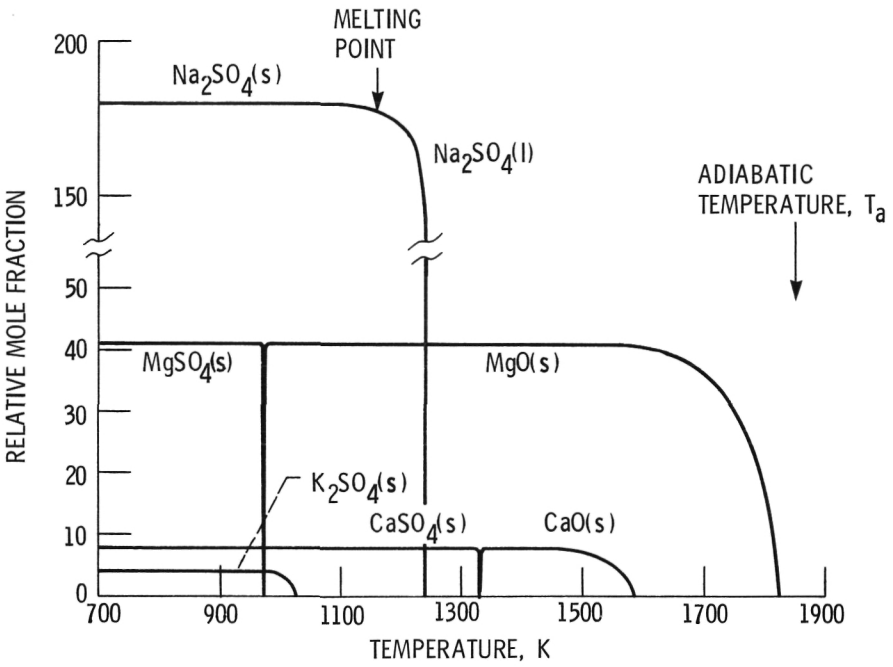

Figure 6. - Relative deposition rates based on the CEC computer programs from synthetic sea salt for all components of the deposit. Note break in the ordinate axis.

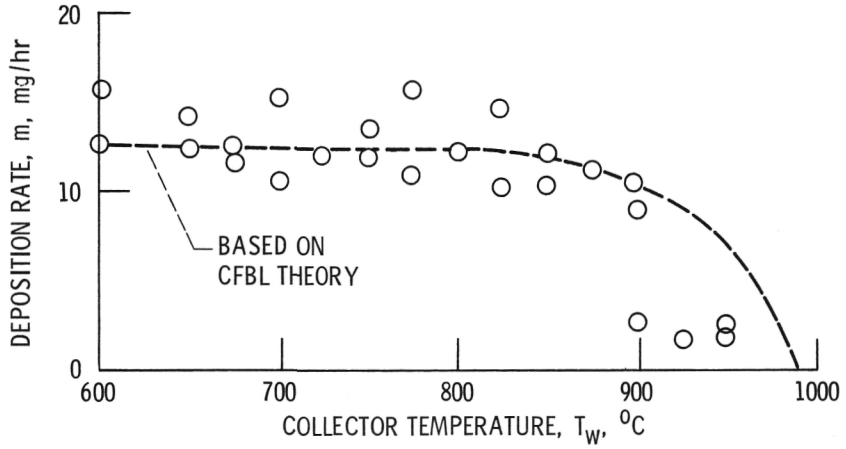

Figure 7. - Effect of collector temperature on deposition rate from NaCl-seeded combustion gases using preheated combustion air. Temperature, 259^0 C.

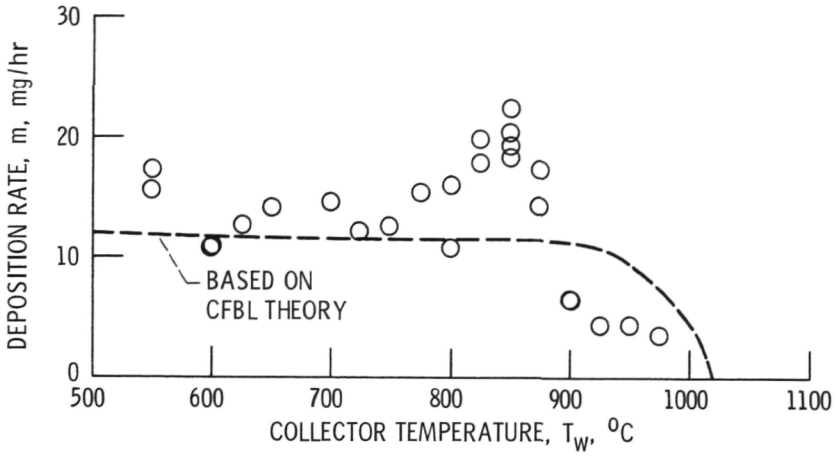

Figure 8. - Effect of collector temperature on deposition rate from $NaNO_3$-seeded combustion gases using preheated combustion air. Temperature, 259^o C.

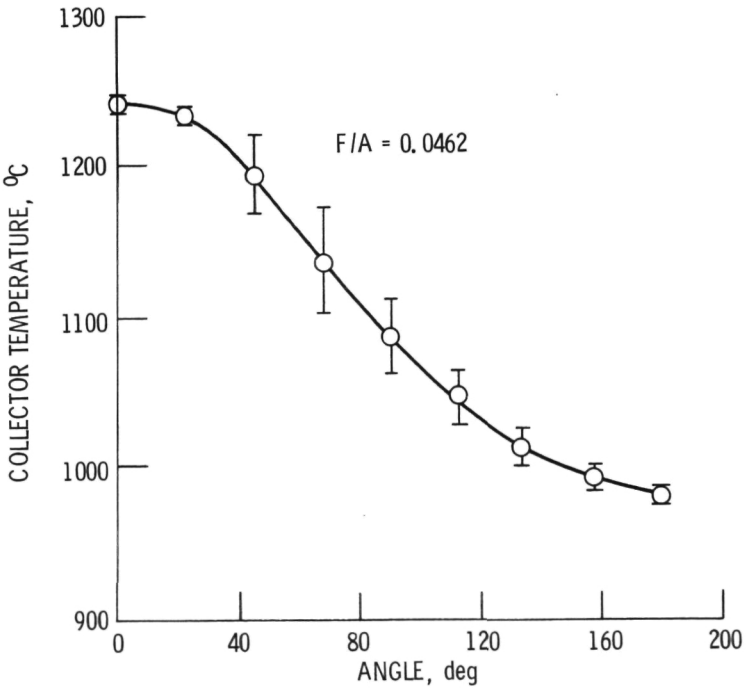

Figure 9. - Temperature distribution on a stationary Pt-Rh collector without internal cooling air. Exposed to unseeded combustion gases.

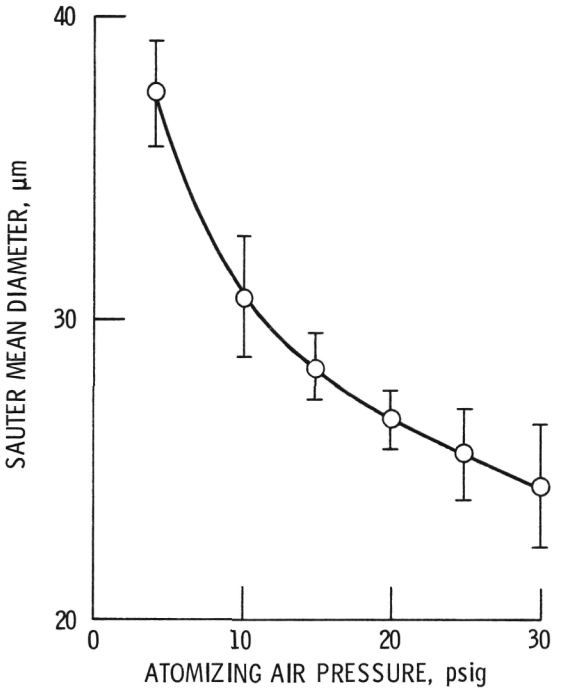

(a) Combined data of distilled water and all the salt solutions SMD as a function of the atomizing air pressure.

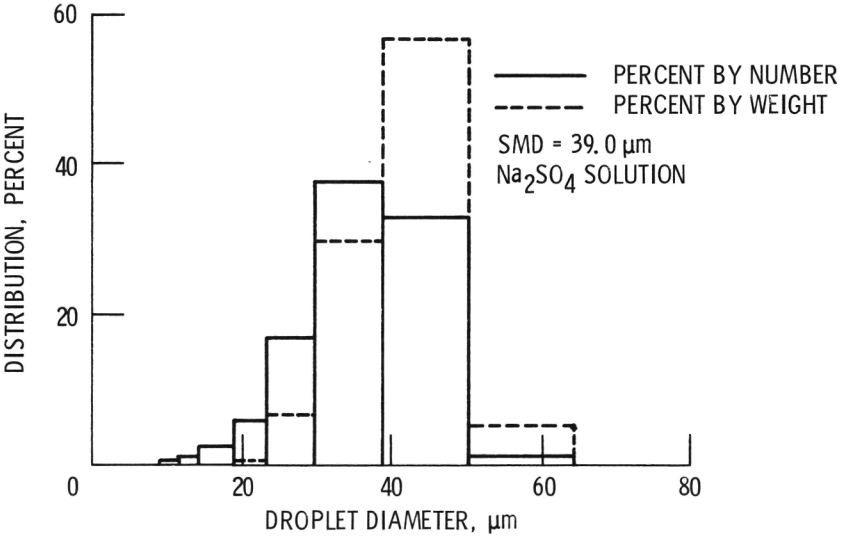

(b) Typical histogram - Na_2SO_4 solution spray droplet size distribution.

Figure 10. - Initial droplet size information.

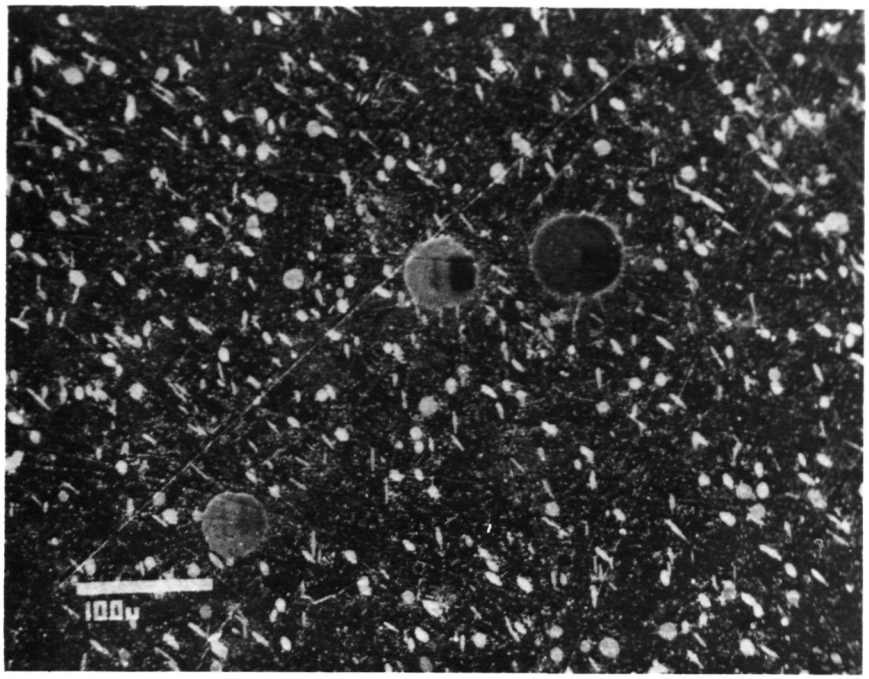

(a) Particles captured from Na_2SO_4 - seeded combustion gases.

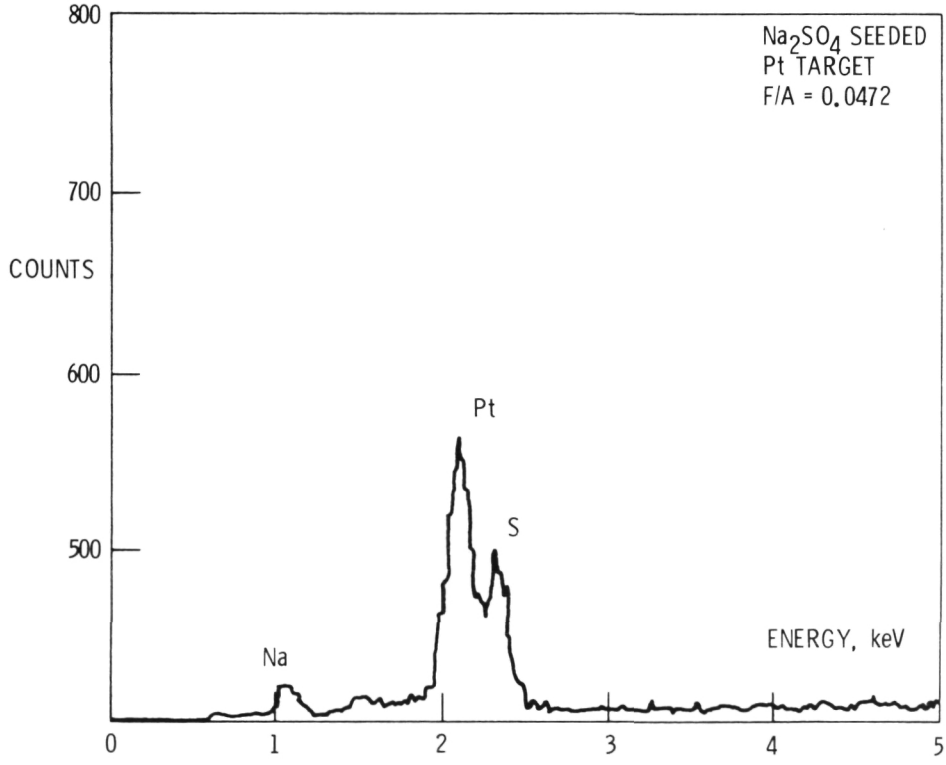

(b) Elements deteced by EDS in particles captured from Na_2SO_4-seeded combustion gases.

Figure 11. - Particle capture results from salt-seeded combustion gases.

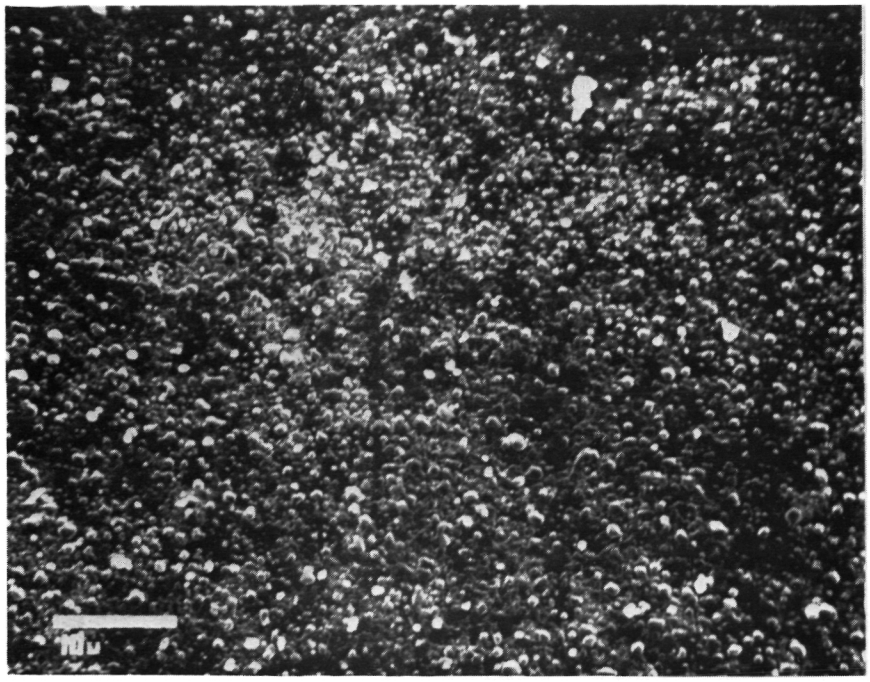

(c) Particles captured from NaCl - seeded combustion gases.

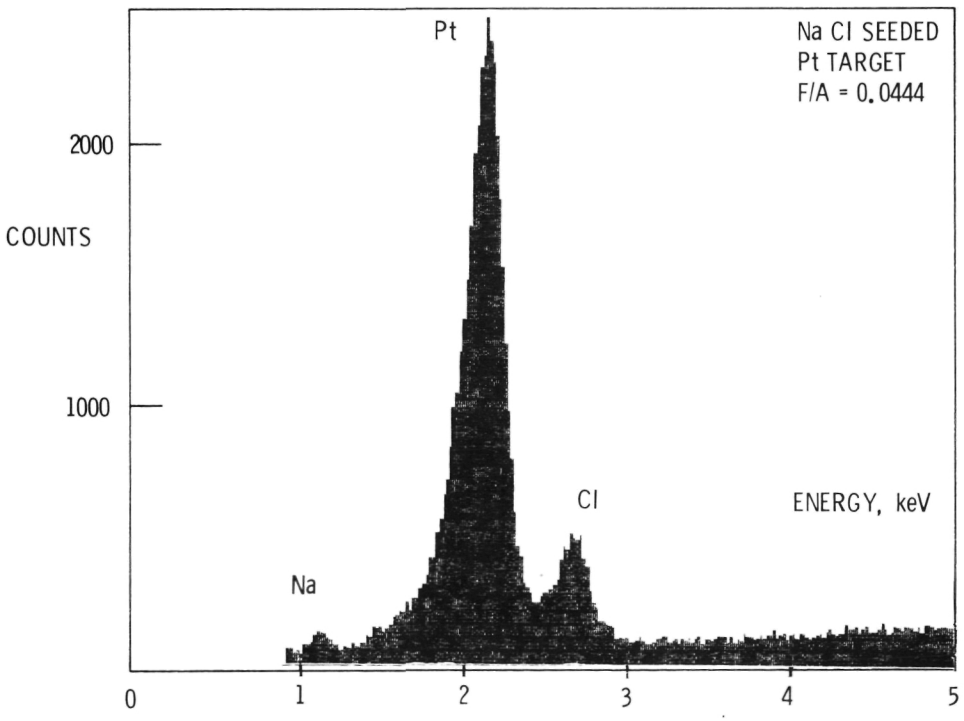

(d) Elements detected by EDS in particles captured from NaCl - seeded combustion gases.

Figure 11. - Concluded.

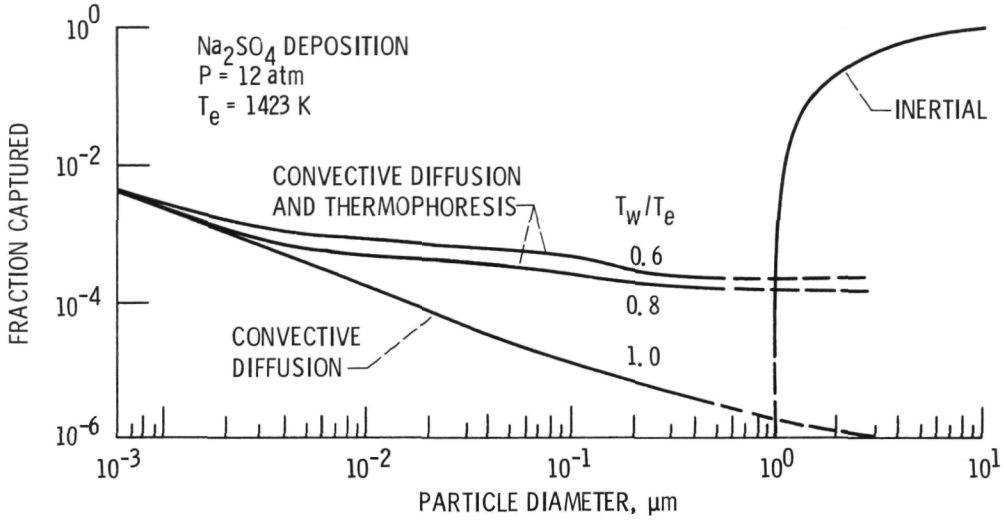

Figure 12. - CFBL theory - predicted deposition rates dependence on particle size and the onset of inertial deposition, from reference 12.

1. Report No.	2. Government Accession No.	3. Recipient's Catalog No.
NASA TM-83751		

4. Title and Subtitle	5. Report Date
Deposition of Na_2SO_4 From Salt-Seeded Combustion Gases of a High Velocity Burner Rig	6. Performing Organization Code: 505-04-1A

7. Author(s)	8. Performing Organization Report No.
G. J. Santoro, S. A. Gökoğlu, F. J. Kohl, C. A. Stearns, and D. A. Rosner	E-2237
	10. Work Unit No.

9. Performing Organization Name and Address	11. Contract or Grant No.
National Aeronautics and Space Administration Lewis Research Center Cleveland, Ohio 44135	13. Type of Report and Period Covered: Technical Memorandum

12. Sponsoring Agency Name and Address	14. Sponsoring Agency Code
National Aeronautics and Space Administration Washington, D.C. 20546	

15. Supplementary Notes

G. J. Santoro, NASA Lewis Research Center; S. A. Gökoğlu, Analex Corporation, Cleveland, Ohio; F. J. Kohl, and C. A. Stearns, NASA Lewis Research Center; D. A. Rosner, Yale University, New Haven, Connecticut 06520. Prepared for the TMS-AIME Fall Meeting, Detroit, Michigan, September 17-19, 1984.

16. Abstract

Under the proper conditions sodium containing contaminants in the combustion air combine with sulfur impurities present in fossil fuels to deposit sodium sulfate on the blades and vanes of the hot section of gas turbine engines. Such deposits cause an accelerated metal wastage termed hot corrosion. The mechanism of deposition of Na_2SO_4 has been studied under controlled laboratory conditions and the results have been compared to a recently developed comprehensive theory of vapor deposition. Thus Na_2SO_4, NaCl, $NaNO_3$ and simulated sea salt solutions were injected into the combustor of a nominal Mach 0.3 burner rig burning jet fuel at constant fuel/air ratios. The deposits formed on inert collectors, rotating in the cross flow of the combustion gases, were weighed and analyzed. Collector temperature was uniform and could be varied over a large range by internal air cooling. Deposition rates and dew point temperatures were determined. Supplemental testing included droplet size measurements of the atomized salt solutions. These tests along with thermodynamic and transport calculations were utilized in the interpretation of the deposition results.

17. Key Words (Suggested by Author(s))	18. Distribution Statement
Deposition Mass and heat transfer Boundary layer Hot corrosion	Unclassified - unlimited STAR Category 34

19. Security Classif. (of this report)	20. Security Classif. (of this page)	21. No. of pages	22. Price*
Unclassified	Unclassified		

*For sale by the National Technical Information Service, Springfield, Virginia 22161

National Aeronautics and
Space Administration

Washington, D.C.
20546

Official Business
Penalty for Private Use, $300

SPECIAL FOURTH CLASS MAIL
BOOK

Postage and Fees Paid
National Aeronautics and
Space Administration
NASA-451

NASA

POSTMASTER: If Undeliverable (Section 158
Postal Manual) Do Not Return